Design of stainless steel homogeneous and hybrid I-sections exhibiting strong flange behaviour

Usman Ali [a*], Gregory Langone [b*], Barbara Rossi [b]
[a] KU Leuven, Belgium; usman.ali@kuleuven.be, barbara.rossi@kuleuven.be.
[b] University of Oxford, England; gregory.langone@new.ox.ac.uk, barbara.rossi@new.ox.ac.uk.
*Co-first authors.

Abstract

Stainless steel built-up I-profile are frequently designed with webs significantly more slender than their flanges, and greater material strength in the flanges in case of hybrid sections. Under the fundamental load case of pure compression or bending, the compressed flange can develop significant post-local-buckling strength, approaching its fully plastic capacity, while the web reaches only its local buckling resistance, a long-overlooked failure mechanism not currently captured by current design approaches. The effect is particularly pronounced in stainless steel, whose nonlinear stress–strain response and pronounced strain hardening further enhance this reserve capacity. In this paper, experiments are first used to validate a finite element model of such behaviour. Following validation, a parametric study is conducted to evaluate the influence of geometric and material parameters on the ultimate strengths. The study includes both homogeneous and hybrid built-up sections, where the homogeneous sections are made of four grades (EN 1.4062, EN 1.4462, EN 1.4307, and EN 1.4404) and the hybrid sections are made using four hybrid combinations – covering a wide range of cross-sectional slenderness. A total of 1325 homogeneous and 955 hybrid FE models are developed, focusing solely on strong flange behaviour. The performance of the codified Effective Width Method, Direct Strength Method, and Continuous Strength Method is evaluated against the numerical results. The comparison highlights that element interaction and local buckling strength reductions cause I-sections with slender webs and stocky flanges to exceed the codified strength predictions. A modified Direct Strength Method (mDSM) approach is then proposed. By introducing two new parameters, Ω and α, to distinguish between cross-sectional behaviours and better account for strong flange effects, we address

Submitted Copy

the limitations of traditional 'whole section' methods while retaining their inherent simplicity, providing greater accuracy and less scatter than any of the codified methods. A reliability assessment provides evidence that the new equation achieves the codified target for acceptable probability of failure when combined with the current resistance factor.

1. Introduction

I-profile members are commonly used in frames as beams, columns, or beam-columns due to ease of connections. The compression behaviour of I-profile members is well understood, specifically in the context of hot-rolled steel. The prevailing design philosophy in hot-rolled section design is often to avoid local buckling entirely using section classification methods based on the width-to-thickness ratios of the member elements [1, 2, 3, 4]. The avoidance of local buckling, however, limits the opportunity to benefit from post-buckling reserve, which can be significant in some sections. Therefore, more materially efficient design typically leads to sections with thinner webs [5], both for members in compression and/or in bending.

While catalogued mild-steel hot-rolled I-profiles generally avoid local buckling, built-up I-profiles with stocky flanges and slender webs can exceed traditional width-to-thickness limits. Research on carbon steel posited that in cases where the I-profile web is more slender than the flanges, it develops only its local buckling capacity while the flanges develop substantial post-buckling reserve strength and approach their full plastic capacity with minimal deformation before failure [6]. This phenomenon is termed ‘strong flange behaviour’. Based on the limited evidence available prior to this paper, the codified forms of the Effective Width Method (EWM) make reasonable, conservative nominal strength predictions for strong flange sections, while the Direct Strength Method (DSM) gives substantially over-conservative nominal strengths [6, 7] leading to uneconomic design.

Submitted Copy

In addition, hybrid I-profile sections – featuring plates of different steel grades welded together – are frequently designed with slender webs and stronger flanges. In 2023, Chen et al. [8] showed that high-strength steel hybrid I-profile sections can be particularly susceptible to strong-flange behaviour. In [9, 10], the first experimental evidence on the behaviour of hybrid structural members under pure bending and combined bending and shear was published. This was followed by [11] in which the first series of tests on hybrid columns was completed. These studies provided the slenderness range in which hybrid columns were more cost-effective than their homogenous counterparts.

However, after these early developments, little to no research was conducted on hybrid members until the early 21st century, when hybrid compression members began to attract renewed attention [8, 12]. The post-buckling behaviour of hybrid sections depends on the most slender plate – typically the web – which governs the overall strength of the cross-section [8]. All the available research and recommendations on hybrid sections were based solely on high-strength steel or carbon steel.

Until recently, no experimental evidence existed for hybrid stainless steel and homogeneous strong flange stainless steel I-sections under compression. In 2025, the same authors conducted the first of its kind experimental work, reported in [13]. The available numerical studies on the hybrid stainless steel [14, 15] remained limited in scope – most notably due to the lack of comprehensive experimental validation. Furthermore, prior numerical research on hybrid stainless steel primarily focused on hybrid combinations within the same stainless steel family, thereby narrowing the range of proof strength difference.

At the same time, the behaviour of stainless steel homogenous I-profiles under strong flange conditions also remained largely unexplored despite clear economic advantages. Given the differences in material properties between stainless and carbon steel – such as the wider strain hardening domain and a nonlinear stress-strain relationship – stainless steel sections

Submitted Copy

may demonstrate even more pronounced post-local-buckling strength reserve and, therefore, have much larger resistance than what any of the codified methods currently account for.

The present study is designed to address these critical research gaps by exploring the local buckling and post-buckling strength reserve in stainless steel I-profiles under compression. Both homogeneous and hybrid stainless steel I-profiles are considered through a comprehensive validated numerical parametric study. Figure 1 shows the overall workflow followed to complete the parametric assessment and develop the new design proposal. Recently completed stub column tests by Langone and Ali et al. [13] enables validation of finite element (FE) models, which are then used to study a wide range of geometric and material parameters influencing the strong flange behaviour. The results of this parametric assessment are subsequently used to propose a modified form of the Direct Strength Method that specifically accounts for the strong flange behaviour of I-profiles. Finally, a reliability assessment is conducted using the numerically generated dataset to compute resistance factors in accordance with AISC 370-21 [3].

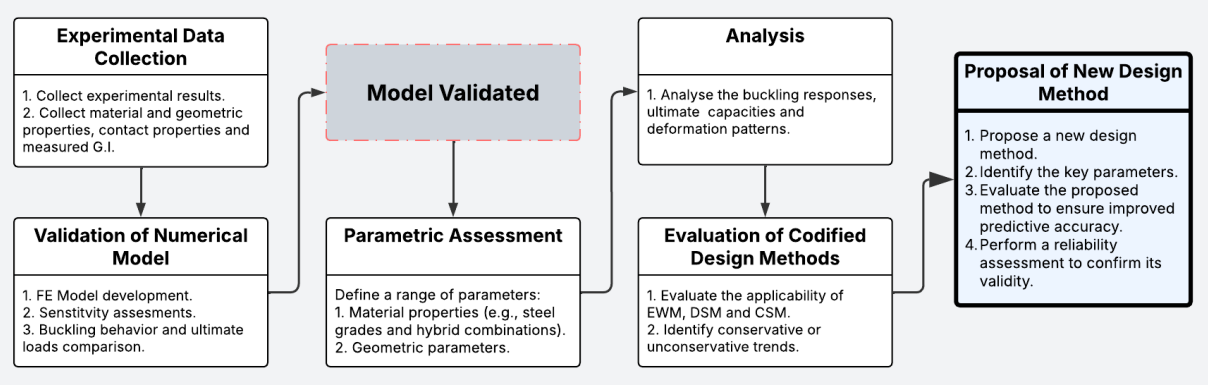


Figure 1. Overview of the parametric study workflow.

1.1. Tests and Design of built-up I-sections

The compression response of stainless steel stub columns has been extensively studied over the last three decades, covering both austenitic and duplex alloys, and multiple cross-section geometries such as I-sections [16, 17, 18, 19, 20, 21], square hollow sections (SHS) [18, 22, 23, 24], rectangular hollow sections (RHS) [22, 23, 25, 26], channel

Submitted Copy

sections [27] and oval hollow sections [28]. The general body of research on stainless steel stub columns contributed to the development of codified design methods such as CSM, DSM, and EWM.

All the previous studies on built-up stainless steel I-sections generally focus on I-profile sections that avoid local buckling entirely or have plates of similar slenderness, i.e., not 'strong flange sections' – termed "conventional" in this paper – and evaluate design methods applicable to that group without consideration of their material efficiency. The only research involving built-up stainless steel I-sections that includes a strong flange configuration is [19], which features one stub column specimen falling in this category among a total of nine specimens tested. While the study assessed both CSM and EWM design methods, test series primarily consisted of conventional I-section geometries. Therefore, the resulting recommendations cannot be considered equally reliable for the strong flange group.

Strong flange I-sections under pure compression were the focus of Rossi and Li's paper in 2013 [6], where they developed a FE model validated on tests of hot-rolled I-section. Ultimate strengths from the FE models were compared with DSM predictions. Rossi and Li identified a distinct difference in the behaviour of sections once a ratio of geometrical dimensions exceeded a critical threshold, termed *LD* for 'limiting dimension'. Sections that exceeded the threshold $LD = \frac{h_w}{t_w}\frac{2t_f}{b_f} > 10.94$ were categorized as exhibiting strong flange behaviour. For I-profiles exhibiting strong flange behaviour, Rossi and Li proposed a simple method to predict the ultimate strength P_u.

The threshold *LD* is especially significant for built-up sections, which often feature slender webs and stocky flanges that go beyond the geometric range of the hot-rolled catalogue sections. While the DSM gave substantially overconservative predictions for

Submitted Copy

sections with LD>10.94, Rossi and Li's equation provided more accurate results. In 2024, Langone et al. [7] researched the initial conceptual development of hybrid configurations and strong flange behaviour under compression. They proposed a modified DSM equation, which was more accurate than Rossi & Li's method based on preliminary evidence. Langone et al.'s method introduced two new parameters: the slenderness ratio (*SlR*) to categorize which sections would exhibit strong flange behaviour, and strength ratio (*StR*) to quantify the magnitude of the effect on ultimate strength.

In 2023, Chen et al. [8] conducted an experimental study on HSS hybrid I-sections, including specimens featuring slender webs and stocky flanges. Additionally, Salem et al. [29] also investigated the post-local buckling strength of carbon steel welded I-profiled sections. Part of their tests focused on pure compression, including sections with strong flanges. They concluded that the web width–to–thickness ratio had a more significant effect on the member capacity compared to the flange width–to–thickness ratios. The test results from [13] were more than doubled the existing body of experimental evidence for strong flange behaviour and provided sufficient evidence to characterize the local buckling mechanisms and plate interactions for these sections. Building up from these experimental results, this paper presents a comprehensive numerical investigation of stainless steel I-profiles exhibiting strong flange behaviour and resolves the long-standing lack of design guidance for such sections.

In addition to the experiments from [13], data was also gathered from the literature, limited to welded I-profile sections under pure compression, as summarized in Table 1 and covers carbon steel, high-strength steel, stainless steel, hybrid high-strength steel, and hybrid stainless steel. Some studies where a full set of nominal and measured section properties could not be obtained were excluded. These experimental results are shown with the

Submitted Copy

numerical results from Section 3.1 in Figures 2 and 4. All gathered data is provided in Appendix to this paper.

Submitted copy

Table 1. Studies containing stub column tests on built-up stainless steel I-sections.

Author	Ref.	Material	Author	Ref.	Material
Chen, 2023	[8]	HSS*	Langone & Ali et. al., 2025	[13]	SS*
Saliba, 2013	[16]	SS	Gardner, 2016	[19]	SS
Yuan, 2015	[20]	SS	Ran, 2022	[21]	SS
Salem, 2005	[29]	CS	Davids, 1989	[30]	CS
Kuwamura, 2003	[31]	SS	Su, 2021	[32]	HSS
Zhou, 2013	[33]	HSS	Rasmussen, 1992	[34]	HSS

CS: Carbon Steel, HSS: High-Strength Steel, SS: Stainless Steel, * includes hybrid sections; different grades in web and flange.

2. Numerical Modelling

The first step of this research was to perform a numerical analysis of built-up I-sections under compression using the commercial finite element analysis (FEA) software ABAQUS 2019 [35], based on the explicit solution procedure. First, a validation model was developed and its results were extensively compared against experimental results in Langone and Ali et al. [13], which include three homogeneous and ten hybrid stub columns, made using carbon steel or stainless steel. The specimens were designed with webs having a significantly higher width-to-thickness ratio compared to the flanges to ensure that strong flange behaviour would be observed in all the cross-sections. The test and detailed development of the validation model were presented by the same authors in [13] including a comprehensive explanation of the mesh sensitivity, boundary conditions, constitutive material models, contact properties, initial geometric imperfections (GI), residual stress, and representation of welds. In the validation, the FE predictions $P_{u,FE}$ were slightly higher than experimental results $P_{u,test}$ with a standard deviation of 0.05. The average experimental-to-numerically obtained ultimate load ($P_{u,test}/P_{u,FE}$) was 0.97 for all thirteen tests.

3. Parametric Study

The parametric study followed the validation of the FE model. It comprised 1325 homogeneous and 955 hybrid simulated stub column tests. The homogenous sections

Submitted Copy

included 560 geometries made of EN 1.4062 and 155 geometries made of EN 1.4462, both grades belonging to the duplex family, as well as 450 geometries made of EN 1.4404 and 155 geometries made of EN 1.4307, i.e. from the austenitic family. Fewer sections were modelled for EN 1.4462 (resp. EN 1.4307), as this grade was shown to lead to nearly the same structural response as sections made of EN 1.4062 (resp. EN 1.4404). Hybrid sections, on the other hand, combined duplex stainless steel in the flanges and austenitic stainless steel or carbon steel in the web. The considered hybrid combinations and the number of modelled sections for each combination are provided in Table 3, which also lists the material and geometric parameters that were varied in the analysis.

Since this research is focused on the local buckling of stub columns, we selected a stub column length of $1.2\,h_w$ as also recommended by Chen et al. [8]. This choice was further verified by evaluating the response of specimens with different column lengths, confirming that, in all cases, failure occurred through local buckling of the web accompanied by plasticity in the flanges, with no global or interactive buckling. For a small subset, a shorted length of 500 mm was used, to ensure that interactive or global buckling would not occur.

The end support conditions were the same as in the validation model, meaning all DOFs were fixed for the rigid plates, except for vertical translation on the top plate. Contact between the column and platens is represented as an ideal fixed-fixed connection by giving coinciding nodes to the elements in contact. In reality, end restraints usually fall between fully fixed and pinned; however, previous studies showed very similar local buckling modes and ultimate capacities in compressed I-profiles with either pinned or fixed end conditions [36]. The increased rotational restraint associated with fixed–fixed conditions slightly reduce global–local interaction effects, resulting in marginally higher ultimate loads than those obtained from pinned stub column models.

Submitted Copy

Unlike the validation models, where end-shortening was measured using strains captured at reference points placed on the outer face of the flange to represent test measurements by a video extensometer, the parametric FE models calculated the end shortening through the vertical downward movement of a reference point defined at the centre of the top rigid plate. This method is ideal for models with a completely fixed contact condition.

The material properties for the parametric study were the nominal material properties per EN 1993-1-1 [37] for carbon steel grade and per [38] for stainless steel, as reported in Table 2. For stainless steel, engineering stress-strain curves were developed using the Ramberg-Osgood equations with the exponent $m = 1 + 2.8 f_u / f_y$ and strain-hardening exponent n from Table 2, as per [38], then converted into true stress-strain curves to implement in Abaqus. For carbon steel, an elastic–perfectly plastic stress–strain curve was developed.

Table 2. Nominal material properties for FE modelling.

Stainless Steel Grade	E	$\sigma_{0.2}$ or f_y	σ_u	**n**
	[GPa]	[MPa]	[MPa]	
EN 1.4062	200	530	700	8
EN 1.4462	200	500	700	8
EN 1.4362	200	450	650	8
EN 1.4307	200	220	520	7
EN 1.4404	200	240	530	7
S355	210	355	490	–

The GI in the parametric assessment models was introduced using the same approach as in the validation model, see [13]. The spatial distribution of imperfection followed the first buckling mode shape obtained through a linear buckling analysis performed for each section using a linear perturbation step with a unit load applied at the reference point on the top rigid plate to extract the buckling mode shapes. The first eigenmode always corresponded to the lowest elastic buckling load. The nodal coordinates associated with the first eigen shape were saved and subsequently imported into the nonlinear static analysis. Following a procedure

Submitted Copy

successfully applied in numerous other studies on steel columns, that shape was scaled up, setting the maximum imperfection in each plate in each section equal to the Eurocode recommended magnitude i.e. the minimum of (*a*, *b*)/200 where *a* is the distance between transverse stiffeners (here the member length, since it is unstiffened) and *b* is plate width [39].

During the validation step, several residual stress models were tested, including the model proposed by Chen et al. [40] for hybrid HSS and the one proposed in prEN 1993-1-14 [41], originally proposed in [42]. Both models were found to provide predictions comparable in terms of initial stiffness loss and ultimate capacity under pure compression. Accordingly, in the parametric analysis, the model from [42] was adopted i.e., residual stresses were modelled as a rectangular stress block distribution, with stress magnitudes defined as functions of the nominal proof strength $\sigma_{0.2}$ and calculated individually for each plate. The complete description of applying the residual stresses is given in [13].

3.1. Numerical Model Results

In selecting the parameters to incrementally change, it was ensured that a wide range of slenderness values with different geometries was considered. A series of sections was developed within which all parameters except for one were kept constant. The primary varied parameter was then studied to capture its effect on the cross-sectional response. In some cases, the ratio $\left(h_w/b_f\right)\vee\left(t_f/t_w\right)$ was the parameter held constant, requiring two parameters to change simultaneously to maintain a constant ratio.

Table 3. Materials and geometries of I-sections included in the parametric study.

	Homogeneous Sections	**Hybrid Sections** (Flange Grade-Web Grade)
Modelled Sections	EN 1.4062 (560 sections) EN 1.4462 (155 sections) EN 1.4404 (450 sections) EN 1.4307 (155 sections)	EN 1.4062-EN 1.4404 (340 sections) EN 1.4062-EN 1.4307 (350 sections) EN 1.4362-EN 1.4404 (110 sections) EN 1.4062-S355 (155 sections)
Geometric Parameters	h_w: [80, 105, 110, 130, 140, 150, 155, 160, 170, 180, 190, 200, 205, 210, 220, 230, 240, 250, 255, 260, 270, 280, 290, 300, 305, 310, 320, 328, 330, 336, 340, 344, 350, 352, 355, 360, 368, 370, 376, 380, 384, 390, 392, 400, 405, 408, 410, 413, 416, 420, 421, 424, 429, 430, 432, 437, 440, 445, 448,	

Submitted Copy

	450, 453, 455, 456, 460, 461, 464, 469, 470, 472, 477, 480, 485, 490, 493, 500, 501, 505, 509, 510, 517, 525, 530, 533, 540, 541, 549, 555, 557, 560, 580, 590, 620, 650, 680, 710] b_f: [60, 70, 80, 90, 100, 0.2h_w, 0.25h_w, 0.3h_w, 0.33h_w, 0.4h_w, 0.45h_w, 0.5h_w,0.55 h_w 0.6h_w] t_w: [3, 4, 5, 6, 8, 9], t_f: [3, 4, 5, 6, 7, 8, 9, 10, 11, 12, 13, 14, 15, 16]

t_w and t_f are the thicknesses of the web and flange respectively, b_f is the width of the flange, h_w is the web height.

Figure 2 depicts the ultimate capacities obtained from numerical models, normalized by their yield loads $P_y = A f_y$ where A and f_y are the gross cross-sectional area and yield strength (or nominal proof strength $\sigma_{0.2}$). For hybrid sections, the effective properties were determined using the weighted average approach (*Eq. 1-2)* to account for hybridity. Here f_u and f_y are ultimate tensile and yield strengths, while A_w and A_f are areas of web and flanges, respectively.

$$f_{y,eff} = \left(A_f f_{y,f} + A_w f_{y,w}\right) / \left(A ¿¿ f + A_w\right) ¿ \quad (1)$$

$$f_{u,eff} = \left(A_f f_{u,f} + A_w f_{u,w}\right) / \left(A ¿¿ f + A_w\right) ¿ \quad (2)$$

The method of using an area-weighted average has been proved efficient in other proposed design methods [14, 15]. Nevertheless, this procedure still needs to be validated, particularly to ensure it accurately represents the strength contributions of materials with highly dissimilar non-linearities. In a worst-case-scenario, a hybrid section made of two metals with markedly different yield strengths could mean that the averaged strength may not be representative of either component, potentially masking early yielding of the weaker element or overstating the contribution of the stronger element. Consequently, further validation is required to identify the limits within which hybrid sections exhibit cohesive cross-sectional behaviour and for which area-weighted averaging remains appropriate.

In Figure 2, the non-dimensional slenderness $\lambda = \sqrt{P_{ne}/P_{cr}}$ is defined per the DSM in AISI S100-16 [43], where P_{cr} and P_{ne} are the section elastic critical buckling load and the global buckling load of the column, respectively. $P_{cr}$is recommended to be computed via the finite strip method (using CUFSM), the FE method, or empirical relations proposed in [44],

Submitted Copy

while P_{ne} is calculated using *Eq. 9*, as described in Section 4.2 of this paper. For all numerical models, P_{cr} was determined through the FE model, whereas for the literature data presented in the Figure 2, P_{cr} was determined based on the critical buckling stress $f_{cr}=k\frac{\pi^2 E}{12(1-v^2)}\left(\frac{t}{h}\right)^2$ of the most slender plate, where the buckling factor k is conservatively taken as 4.0 for internal compression members and 0.43 for outstand elements and v is the Poisson's ratio of the plate material.

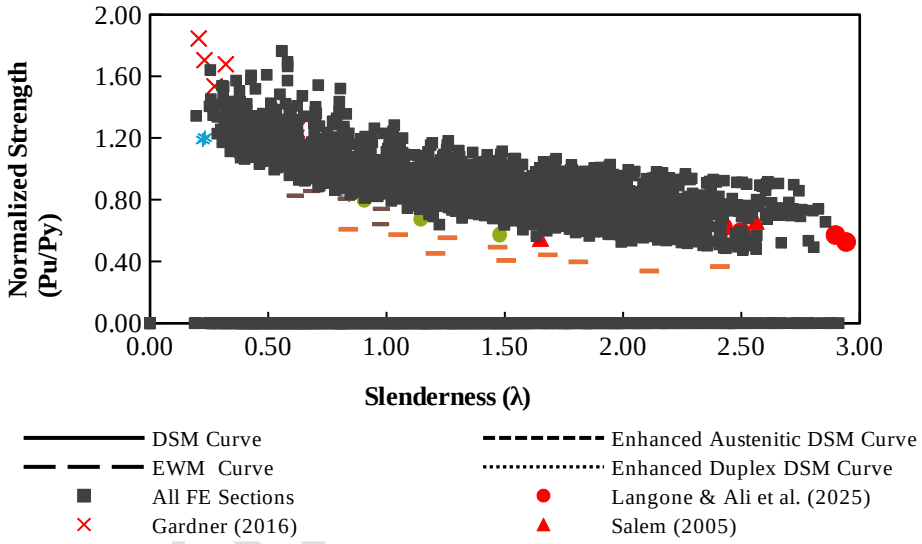


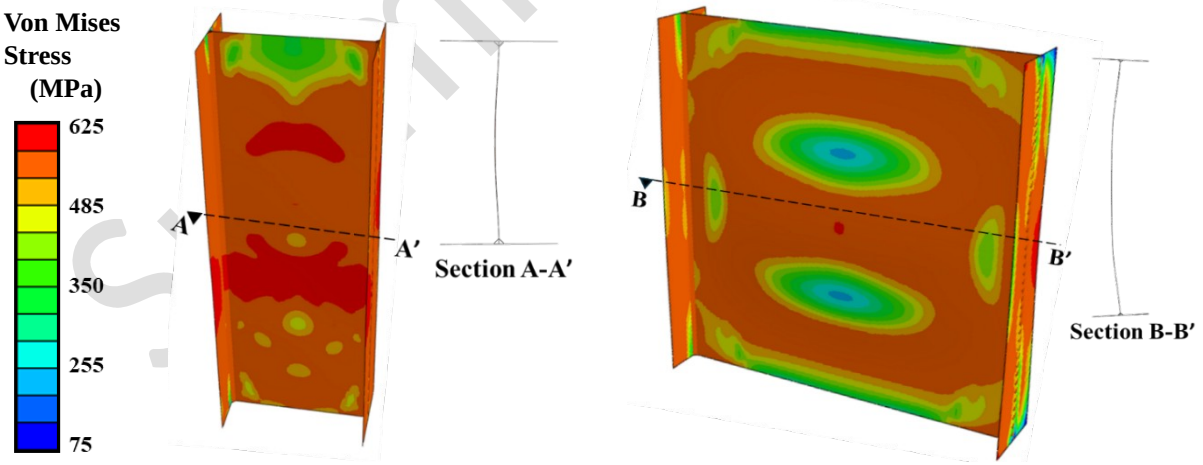
Figure 2. Normalized strength (P_u/P_y) versus slenderness results from literature experiments or from the FE model parametric assessment (all 2280 FE models represented).

Figure 2 presents the FE and literature dataset as per Table 1, along with four curves: the DSM curve based on *Eq. 9-10*, the EWM curve from *Eq. 6-8*, and the enhanced DSM curves proposed for duplex and austenitic stainless steel in [45], which account for the strain hardening effects of stainless steel. The scattered nature of the data for $\lambda>0.776$ can be attributed to two distinct behaviours of the stub columns. The variation in prediction accuracy for these two groups is attributed to their modes of failure, reinforcing their categorization into two distinct groups. Section 3.2 provides a detailed procedure to define the appropriate

Submitted

parameters for categorizing these sections into the two distinct groups, see Figure 4 later in the paper.

Figure 3 shows two typical behaviours observed in the FE study: Section I-460×100×12×6 which exhibits strong flange behaviour and Section I-160×100×12×6 which exhibits a compression response governed by yielding. Both cross-sections are made up of lean duplex stainless steel EN 1.4062 with a nominal yield strength of 530 MPa. Figure 3 shows the Von Mises stress distribution in these two sections at their respective ultimate strengths $P_{u,FE}$. In section I-160×100×12×6, most of the flanges along with a significant portion of the web have yielded at $P_{u,FE}$ reaching stresses greater than 530 MPa. Additionally, P_{cr} is significantly higher than both $P_{u,FE}$ and P_y, local buckling does not occur in the elastic range and is not governing failure. Instead, the section undergoes plastic deformation, with its capacity limited by material yielding. Most importantly, the web, being the most slender element in cross section, does not buckle before the ultimate load is reached. The section cut A-A' shows minimal deformation at mid-span at the point of ultimate strength.



a) I-160×100×12×6
δ = 2.86 mm (at P_u)

b) I-460×100×12×6
δ = 2.06 m (at P_u)

Figure 3. Schematic of Von Mises stresses for two sections under compression at P_u.

In Section I-460×100×12×6, by contrast, the flange yields while large portions of the web fail to reach 530 MPa. Local buckling of the web initiates when the critical local

Submitted Copy

buckling web capacity is reached,after which the section exhibits post-buckling reserve and partial yielding develops in the cross-section. However, web local buckling prevents fully plastic behaviour, resulting in an ultimate load capacity noticeably lower than P_y. Despite this, stainless steel's superior ductility and large strain hardening domain compared to carbon steel lead to a pronounced strong-flange effect, enabling greater post-buckling reserve to sustain additional load beyond the critical elastic buckling point. At higher end-shortening values, a larger portion of the web has yielded, accompanied by further plastification and rotation of the flanges in opposite directions. This behaviour differs notably from that of the first case, suggesting that a unified classification may result in overly conservative predictions.

It is important to note that plate strength reductions due to local buckling are well described and quantified, for example, in the EWM. Strong flange behaviour of I-sections is therefore of greatest concern when “whole-section” or “non-dimensional” slenderness definitions are used, like it is the case for the DSM and CSM. On the other hand, it is necessary to have sufficiently simple design equations that enable a labour-efficient design process to unlock structural gains at design stage. Thus, it is a priority to consider how methods like the DSM (and CSM) can be adapted to maintain design simplicity without overlooking the important advantages of sections exhibiting strong flange behaviour.

The key distinction between existing methods and the observed behaviour of I-460×100×12×6 lies in its ability to reach higher ultimate forces despite undergoing local buckling. This is caused by two factors. Firstly, the development of stresses beyond f_y thanks to strain hardening in compact flanges, and potentially in portions of the buckled web, is occurring. Secondly, strong flanges provide restrained end conditions to the web (closer to ideal fixed end conditions rather than a pinned end assumption [5, 44]) which increases its buckling resistance beyond design predictions. This case of element interaction is not

Submitted copy

accounted for in the EWM. Design methods that treat plate strengths independently fail to capture the interactive effects, which are particularly pronounced in I-sections with strong flanges. On balance, however, accounting for the slenderness-induced instabilities of individual plates has a significantly greater impact on predicting strength than accounting for element interactions.

The remainder of this paper, therefore, aims to develop a modification to the DSM that quantifies the capacities of strong flange I-sections. This modification will maintain the simplicity of the 'whole cross-section approach' (the primary motivation for its development), will account for plate slenderness instabilities as the EWM precisely, and will provide an opportunity to account for element interactions.

3.2. Development of the Strong Flange Parameters

To address the limitation of the DSM, two parameters, κ and Ω, given in *Eq. 3* and 4, are introduced to classify strong flange sections and allow to adjust their strength predictions accordingly.

$$\kappa = \frac{t_f b_f}{t_w h_w} \lambda_l^2 = \alpha \lambda_l^2 \tag{3}$$

$$\Omega = \left(\frac{h_w}{t_w} \sqrt{f_{y,f}} \right) / \left(\frac{(b_f - t_w)}{2 t_f} \sqrt{f_{y,w}} \right) \tag{4}$$

where $\lambda_l = \sqrt{P_{ne} / P_{crl}}$ is the cross-sectional slenderness defined for the cases governed by local buckling and the other variables take their usual meaning.

In Section 3.1, an extensive range of material and geometric parameters was investigated to best capture the strong flange behaviour effect on ultimate strength of built-up I-profile stub columns. Based on this analysis, it was established that two fundamental effects combine to produce strong flange behaviour: strength reductions due to slenderness instability and elements interaction.

Submitted Copy

The parameter κ is derived starting from the first premise that strong flange behaviour will be more pronounced in sections where there is a large difference between the strengths of each plate, hence it evaluates the ratio between the ultimate strength of the flange and that of the web. The theoretical approach followed in [6] postulates that strong flange sections develop full yield capacity in the flange and only the critical elastic buckling capacity in the web. This hypothesis is further supported by the analysis of the EWM strength predictions for web and flange plates composing strong flange sections. The numerical evidence given in Section 3.1 confirms that this prediction is a reasonable basis for the approximation of the ultimate strengths in sections with strong flanges. To incorporate this parameter into the DSM, the flange yield stress $f_{y,f}$ is conservatively approximated as the column global compressive stress f_{ne}, as calculated by the DSM. This enables algebraic manipulation to express this ratio in terms of λ_l and a new geometric parameter α, defined as a combination of four geometric dimensions, as summarized in *Eq. 5*.

$$\frac{Flange\ Strengt\ h}{Web\ Strengt\ h} \approx \frac{f_{y,f} t_f b_f}{\sigma_{cr,w} t_w h_w} \approx \frac{t_f b_f}{t_w h_w} \frac{f_{ne}}{f_{crl}} = \frac{t_f b_f}{t_w h_w} \lambda_l^{\,2} = \alpha \lambda_l^{\,2} = \kappa \tag{5}$$

When ratio of numerically computed strength-to-DSM predicted strength ($P_{u,FE}/P_{DSM}$) is plotted against κ, two separate clusters of points are distinguished, see Figure 7. The upper nonlinear cluster corresponds to strong flange sections and shows a direct relationship between $P_{u,FE}/P_{DSM}$ and κ. The lower cluster shows weaker trend and corresponds to more conventional I-section shapes that avoid local buckling or have plates of similar slenderness.

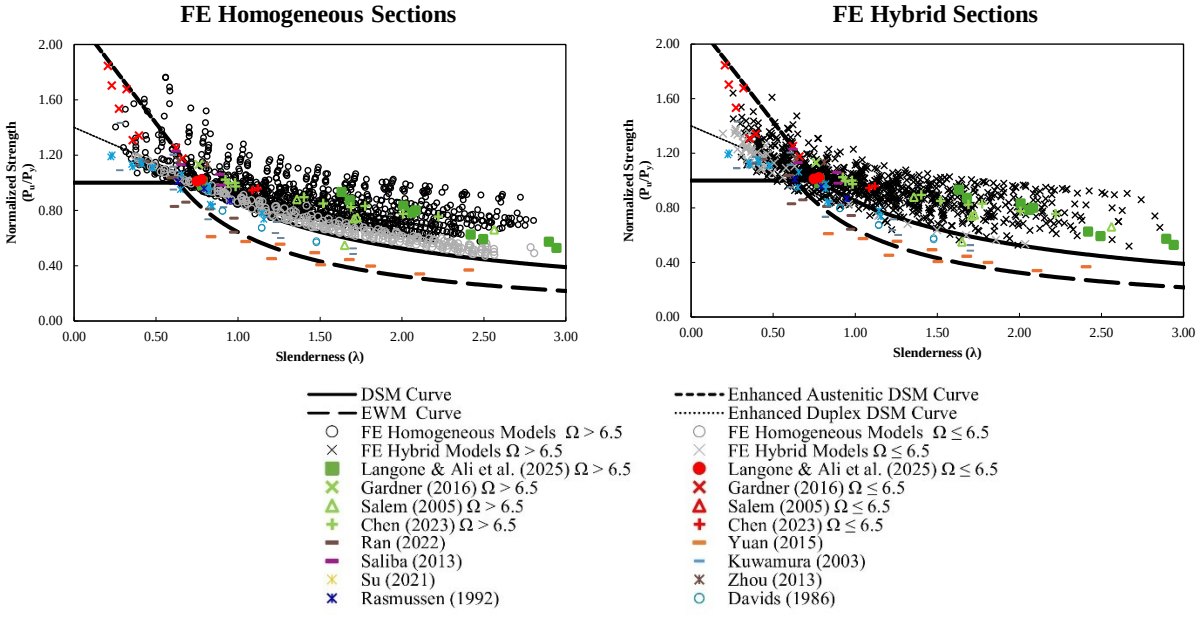
The parameter Ω was developed to segregate these two clusters of points. The basis for finding Ω lays in those sections with plates of similar slenderness will not exhibit strong flange behaviour. The parameter Ω should provide a comparison of the web and flange slenderness. In general, plate slenderness is defined as width-to-thickness ratio multiplying $\sqrt{f_y/E}$ which comes from a non-dimensional form of the critical buckling stress equation for

Submitted Copy

plates. Thus, Ω is chosen as the ratio of the web height-to-thickness ratio divided by the square root of web yield strength to the same for the flange. Algebraically rearranged for simplicity, Ω is defined by *Eq. 4*.

A preliminary threshold of $\Omega=6.5$ was selected by visual inspection as the basis for further analysis. As seen in Figure 7, the $\Omega=6.5$ threshold is very successful at classifying which sections may exhibit strong flange behaviour. With the κ and Ω parameters defined, section 4.4.1 addresses incorporating these parameters into a modified DSM equation

Figure 4 presents the same dataset as Figure 2, but segregated to separately display the FE homogeneous and FE hybrid sections. Each group is further divided into two groups based on the Ω threshold of 6.5, with $\Omega>6.5$ classified as exhibiting strong flange behaviour. The strong-flange sections lie substantially above the codified DSM curve (i.e. over-conservative predictions). Figure 4 also includes the literature data points alongside the FE dataset. The literature data contains a few cross-sections demonstrating strong flange behaviour; the primary sources are two papers [8, 29], both focusing on high-strength or carbon steel and our paper [13] which recently added experimental evidence to the strong flange behaviour of stainless steel cross-sections.



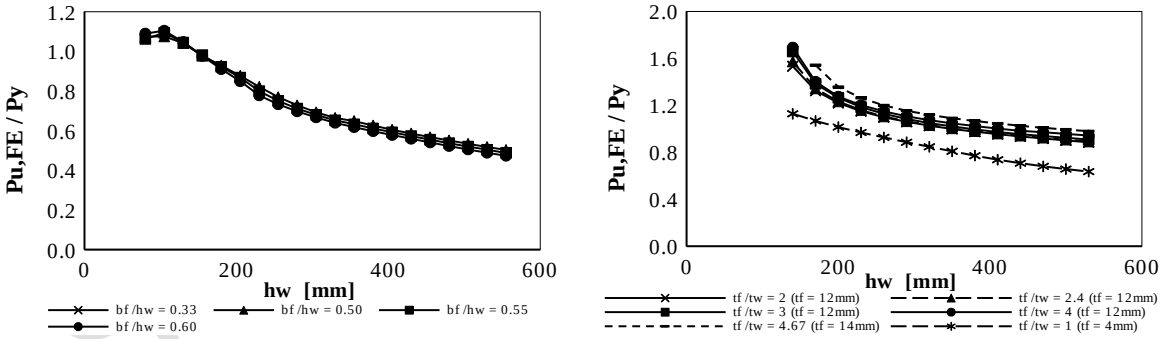
Submitted Copy

Figure 4. Normalized strength (P_u/P_y) versus slenderness (split by $\Omega=6.5$)

3.3. Effect of geometric parameters on ultimate capacity

The local slenderness of the plates has a pronounced effect on the overall capacity of the cross-section. Increasing web height h_w increases the gross-section capacity P_u, but reduces the normalized capacity $P_{u,FE}/P_y$ due to the associated increase in web local slenderness (h_w/t_w ¿ which promotes earlier local buckling and prevents full cross-sectional plastification, as shown in Figure 5(a). While larger flange-to-web width ratios b_f/h_w provide some mitigation, the reduction in normalised capacity with increasing h_w remains dominant.

By contrast, increasing the flange-to-web thickness ratios (t_f/t_w) provided greater rotational restraint at the web-flange junction, significantly enhancing the post-buckling resistance. This results in consistently higher values of $P_{u,FE}/P_y$ across the whole range of web heights, see Figure 5(b). The improvement observed for larger t_f/t_w ratios highlight the critical role of flange stiffness in activating the strong flange behaviour.



(a) Influence of b_f/h_w variation (b) Influence of t_f/t_w variation

Figure 5. Geometric parameters versus normalized capacity.

4. Assessment of Current Design Methods and Development of New DSM Equation

In this section, the applicability of three codified design methods, including EWM, DSM, and CSM, is assessed for FE dataset of stub columns alongside a modified form of DSM.

Submitted Copy

4.1. Effective Width Method

The EWM is widely accepted in international design standards [1, 2, 3, 4] where the cross sections are classified based on the width-to-thickness ratio of each plate comprising it, i.e. their propensity to be subject to local buckling. In this paper, the EWM from prEN 1993-1-4:2023 is assessed. For non-slender cross-sections, the ultimate capacity is $P_{u,EWM} = A f_y$. For slender sections (Class 4), a reduction factor ρ which accounts for local buckling by reducing the gross cross-sectional area to an effective area $A_{eff} = \rho A$ is considered. The reduction factor ρ depends on the plate slenderness and stress distribution. *Eq. 7-8* are used to determine reduction factor ρ for welded internal and outstand plates.

λ_p is the plate slenderness:

$$\lambda_p = \sqrt{\frac{f_y}{f_{cr}}} = \frac{\frac{b}{t}}{27.7\,\varepsilon\sqrt{k}} \tag{6}$$

For internal compression elements:

$$\rho = \begin{cases} 1.0 \; if \; \lambda_p \le 0.328 + \sqrt{0.100 - 0.003\Psi} \\ \dfrac{0.655\,\lambda_p - 0.003(3+\Psi)}{\lambda_p{}^2} \le 1.0 \; if \; \lambda_p > 0.328 + \sqrt{0.100 - 0.003\,\Psi} \end{cases} \tag{7}$$

For outstand compression elements:

$$\rho = \begin{cases} 1.0 \; if \; \lambda_p \le 0.639 \\ \dfrac{0.655\,\lambda_p - 0.01}{\lambda_p{}^2} \le 1.0 \; if \; \lambda_p > 0.639 \end{cases} \tag{8}$$

where $\varepsilon = \sqrt{235/f_y}$ is the material coefficient, b and t are the width and thickness of the considered plate, and Ψ is the stress ratio based on loading and boundary conditions.

The EWM performance is evaluated by comparing its predictions against the numerically obtained compression capacities, as presented in Figure 6(a). The EWM is typically accurate but slightly conservative for predicting the capacity of strong flange cross-sections. The average normalized capacity $P_{u,FE}/P_{EWM}$ for the strong flange group is predicted approximately 20.5% more accurately than for the conventional I-section group,

Submitted copy

with a coefficient of variation (CoV) of 0.083 (compared to the 0.187 for conventional I-section), which, despite the conservative bias, reflects less scatter and more uniformity in the predictions. The overall conservative nature of the Eurocode predictions is partly because it does not allow strengths to exceed the yield capacity.

4.2. Direct Strength Method

DSM was introduced to design cold-formed steel (CFS) sections exhibiting local, distortional or global buckling or a combination of those [46]. Unlike the EWM, the DSM proposes that members ultimate strengths be represented as a direct function of the nominal yield strength and the cross-section slenderness for the relevant buckling mode, see *Eq. 9-10*. If one failure mode is not present under specific loading conditions, then it is ignored in design [47]. Therefore, the distortional buckling mode is not considered herein. In the DSM equations, λ_G and λ_l are the global and local buckling slenderness, P_{cre} and P_{crl} are the capacities under elastic critical global buckling and local buckling, and P_{ne} and P_{nLG} are the global buckling capacity and the combined local-global buckling capacity, respectively. The elastic critical global buckling load P_{cre} is determined from the analytical expression $\pi^2 EI/(KL/r_y)^2$ where K is the effective length factor, E is the modulus of elasticity, r_y is the minimum radius of gyration, and L is the length of the column.

$$P_n = min(P_{ne}, P_{nLG})$$

$$\frac{P_{ne}}{P_y} = \begin{cases} 0.658^{\lambda_G^2} \, if \, \lambda_G \le 1.5 \\ 0.877^{\lambda_G^{-2}} \, if \, \lambda_G > 1.5 \end{cases} \quad \lambda_G = \sqrt{\frac{P_y}{P_{cre}}} \tag{9}$$

$$\frac{P_{nLG}}{P_{ne}} = \begin{cases} 1.0 \, if \, \lambda_l \le 0.776 \\ \left(1 - 0.15\,\lambda_l^{-0.8}\right)\lambda_l^{-0.8} \, if \, \lambda_l > 0.776 \end{cases} \quad \lambda_l = \sqrt{\frac{P_{ne}}{P_{crl}}} \tag{10}$$

Figure 6(b) shows that the average ratio $P_{u,FE}/P_{DSM}$ for conventional I-sections is 21.6% more accurate than for those with strong flanges. Significant variation is observed in

Submitted Copy

the prediction accuracy for strong flanges sections. The CoV for the strong flange section group is 0.19, which is 175% higher than that of the conventional group.

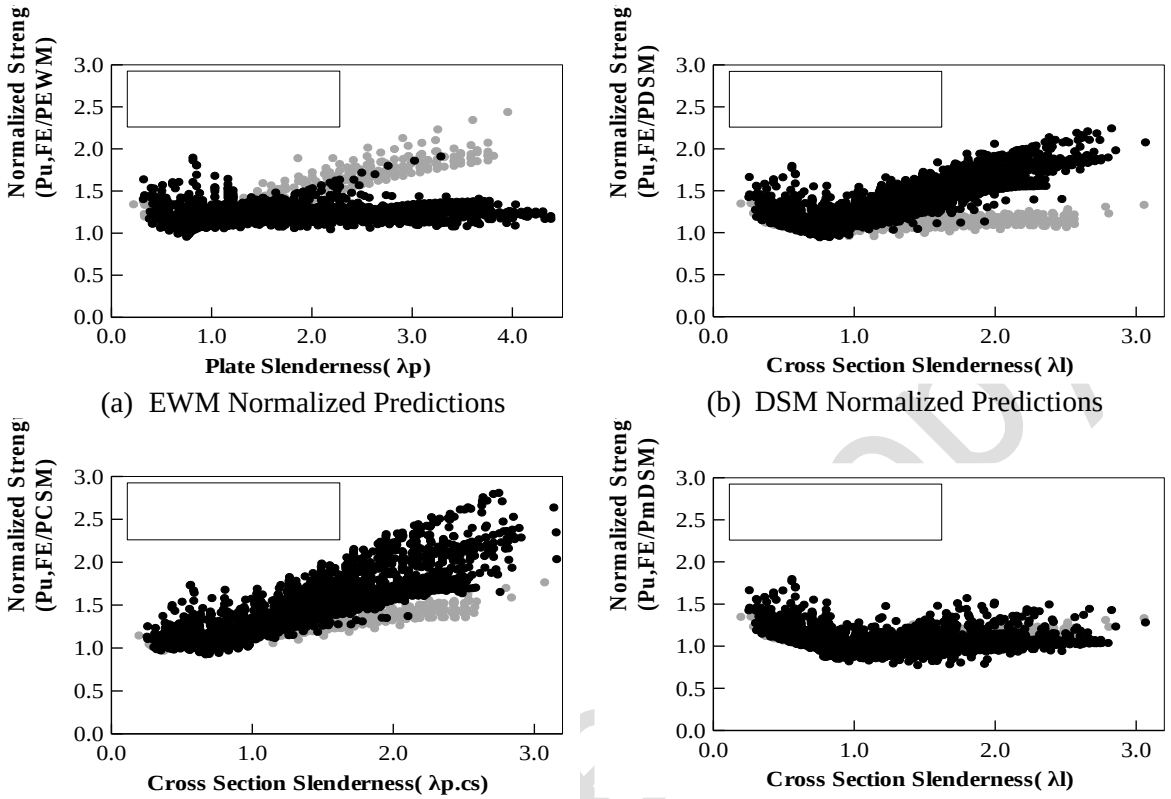


Figure 6. Normalized FE model to design method strengths versus slenderness.

Table 4 compares the numerically computed strengths, normalised by the predictions from the DSM and EWM approaches. For the full dataset, the average values are relatively close. However, in the strong flange group, the EWM yields an average ratio of 1.23, compared to 1.38 for the DSM, indicating that the DSM is overly conservative for this case. In contrast, for the conventional I-section group, the EWM proves too conservative.

4.3. Continuous Strength Method

CSM is a deformation-based design method that was introduced in 2008 [48] to capture the continuous resistance predictions across varying stainless steel cross-section slenderness. It is comprised of two main components, a base curve to determine the cross-section deformation capacity ε_{csm} and a constitutive material model. The codes [49, 1]

Submitted

propose two different equations for the base curves, one to use in conjunction with a bi-linear material model and the other to use in conjunction with the two-stage Ramberg-Osgood material model.

Unlike the EWM, the CSM considers the effects of strain hardening and element interaction to predict the ultimate capacity of stainless-steel compression members. Various researchers have applied the CSM to the design of slender and non-slender stainless-steel section [50, 51, 52, 53]. The relationship between the cross-sectional slenderness $\lambda_{p,cs}=\sqrt{P_y/P_{cr}}$ and the normalized deformation capacity $\varepsilon_{csm}/\varepsilon_y$ is given by *Eq. 11*. Importantly, the CSM slenderness $\lambda_{p,cs}$ is different than the DSM slenderness λ_l as the CSM uses P_y in the numerator, while the DSM uses P_{ne} (determined by *Eq. 9*) in the numerator. The cross-sectional compression resistance P_{CSM} is determined by *Eq. 12-13*.

$$\frac{\varepsilon_{csm}}{\varepsilon_y}=\begin{cases}\dfrac{0.25}{\lambda_{p,cs}^{3.6}}\le min\left(15,\dfrac{C_1\varepsilon_u}{\varepsilon_y}\right) & \lambda_{p,cs}\le 0.68\\ \left(1-\dfrac{0.222}{\lambda_{p,cs}^{1.050}}\right)\dfrac{1}{\lambda_{p,cs}^{1.050}} & \lambda_{p,cs}>0.68\end{cases} \tag{11}$$

$$f_{csm}=f_y+E_{sh}\varepsilon_y\left(\frac{\varepsilon_{csm}}{\varepsilon_y}-1\right) \tag{12}$$

where the strain hardening modulus E_{sh} ¿ $\dfrac{f_u-f_y}{C_2\varepsilon_u-\varepsilon_y}$, with $\varepsilon_u \wedge \varepsilon_y$ being the strains at ultimate and yield strengths, respectively. For austenitic and duplex stainless steel grades, the constant C_1 is taken as 0.1 and the constant C_2 as 0.16. For carbon steel, $C_1$and C_2 are taken from [54] where C_1=¿, C_2=¿ and $\varepsilon_{sh}=0.1\dfrac{f_y}{f_u}-0.055$ subject to the bounds $0.015\le\varepsilon_{sh}\le 0.03$. For hybrid sections, the weighted average values of E_{sh}, f_u, ε_u, ε_y and f_y are used.

Submitted Copy

$$P_{CSM}=\begin{cases}\dfrac{\varepsilon_{csm}}{\varepsilon_y}Af_y\dfrac{\varepsilon_{csm}}{\varepsilon_y}<1\\ Af_{csm}\dfrac{\varepsilon_{csm}}{\varepsilon_y}\geq 1\end{cases} \quad (13)$$

Figure 6(c) indicates that the current form of the CSM is more conservative than either the EWM or DSM when predicting the capacities of the given dataset yet accurately predicts the strength of more conventional cross-sections.

When the two groups (strong flange group and not strong flange group) are examined separately in Figure 6(c), the CSM provides more accurate predictions for conventional sections in the low slenderness range, while it becomes overly conservative for those characterised by strong flange behaviour. The CoV for strong flange sections is 0.25, almost double that of the conventional I-section group, indicating greater variability and significantly more conservative strength predictions.

Table 4. Numerically computed strengths divided by nominal strengths from four design methods.

Normalized Predictions	Sections	Sample Size			Average			CoV		
		All	Homo.	Hybrid	All	Homo.	Hybrid	All	Homo.	Hybrid
$\frac{P_u}{P_{EWM}}$	$\Omega\leq 6.5$	290	244	46	1.54	1.59	1.27	0.19	0.17	0.14
	$\Omega>6.5$	1990	1081	909	1.23	1.26	1.18	0.08	0.08	0.07
	All	2280	1324	955	1.27	1.32	1.19	0.15	0.15	0.08
$\frac{P_u}{P_{DSM}}$	$\Omega\leq 6.5$	290	244	46	1.13	1.12	1.12	0.07	0.06	0.10
	$\Omega>6.5$	1990	1081	909	1.38	1.40	1.35	0.19	0.18	0.20
	All	2280	1324	955	1.35	1.35	1.34	0.19	0.19	0.19
$\frac{P_u}{P_{CSM}}$	$\Omega\leq 6.5$	290	244	46	1.26	1.29	1.06	0.13	0.12	0.06
	$\Omega>6.5$	1990	1081	909	1.47	1.53	1.41	0.25	0.24	0.25
	All	2280	1324	955	1.44	1.48	1.39	0.24	0.24	0.26
$\frac{P_u}{P_{mDSM}}$	$\Omega\leq 6.5$	290	244	46	1.13	1.12	1.18	0.07	0.06	0.10
	$\Omega>6.5$	1990	1081	909	1.07	1.03	1.12	0.12	0.11	0.12
	All	2280	1324	955	1.08	1.05	1.12	0.11	0.11	0.12

4.4. Modified DSM Proposal

As observed in Section 4.2, the DSM in its current codified form, does not adequately capture the distinct behaviour of strong flange sections. Overconservative DSM predictions have been addressed in multiple previous instances [14, 45]. These modifications, however, focus on sections in the low slenderness range and provide no basis to explain why, for

Submitted Copy

example, a section with high cross-section slenderness (e.g. λ_l=2) and thick flanges may develop a strength 60% greater than the DSM prediction. Therefore, a modification is proposed to enhance the DSM predictive performance based on the two key parameters κ and Ω as previously defined in Section 3.2.

4.4.1. Development of mDSM

The relationship between $P_{u,FE}/P_{DSM}$ and κ was quantified to establish an empirically derived correction function $g(\alpha,\lambda_l)$ for the strength prediction of strong flange I-sections. The modified DSM general form, given in *Eq. 14*, reflects the approach that for sections which may exhibit strong flange behaviour (Ω>¿threshold), the current DSM prediction should be multiplied by this function $g(\alpha,\lambda_l)$. As shown in *Eq. 5*, α and λ_l parameters are directly linked to the ratio between the yield strength of the flanges and the critical buckling strength of the web. In sections where the flange's strength greatly exceeds that of the web, the flanges provide more rotational restraint to the web, thereby effectively increasing the buckling capacity of web. Incorporating a mathematical function $g(\alpha,\lambda_l)$ into the modified DSM allows the design method to account for this additional rotational restraint.

$$P_{nLG}=\begin{cases} ¿\,if\ \lambda_l \le 0.776\, P_{ne} \\ ¿\,if\ \lambda_l>0.776 \begin{cases} \left(\lambda_l^{-0.8}-0.15\,\lambda_l^{-1.6}\right)P_{ne}\ if\ \Omega \le Threshold \\ \left(g(\alpha,\lambda_l)*\left(\lambda_l^{-0.8}-0.15\,\lambda_l^{-1.6}\right)\right)P_{ne} \le P_y\ if\ \Omega>Threshold \end{cases} \end{cases} \quad (14)$$

$$g(\alpha,\lambda_l)=1+\frac{0.42\,\alpha^{0.6}\,\lambda_l^{1.2}}{1+0.04\,\alpha\,\lambda_l^{2}} \quad (15)$$

The dataset for this empirical analysis was the population of the 1325+955 (Homogeneous+ hybrid) numerically modelled stub columns for which Ω>6.5 (i.e., those which exhibit strong flange behaviour). The *y*-intercept for the relationship was forced through 1.0 (i.e. $P_{u,FE}$=P_{DSM}¿. Ten different equations forms were considered as potential best representations of the data. In all equations, the coefficients are determined by the least

Submitted copy

511 squares regression. Table 5 provides the considered function $g(\alpha,\lambda_l)$and their design
512 performance.

513 Expectedly, the first tested equations explicitly model saturating exponential behaviour,
514 of the form $1+C_1(1-e^{-C_2\kappa})^{C_3}$, where C_1, C_2 and C_3 are constants to be determined, modelling
515 a response that starts at 1 when $\kappa=0$and increases non-linearly, flattening out as κ increases.
516 The first three in the dataset, labelled with "LB", contain numerical parameters which were
517 fit to a collection of points identified at 0.1 intervals along the x-axis forming the lower
518 bound of the strong flange data cluster. Consequently, they have inferior fitting i.e., negative
519 R^2 values when tested against the full dataset, but fewer unconservative predictions, contrary
520 to the next three equations, whose numerical parameters were fitted based on their adequacy
521 against the full strong flange dataset. The last four equations are simplified mathematical
522 approximations, surrogates designed to start at (or near) 1, increase with κ, and asymptote in
523 a similar way, even if not through an exact exponential mechanism.

524

Submitted Copy

Table 5. Evaluation of correction factor equations based on data fit and design performance.

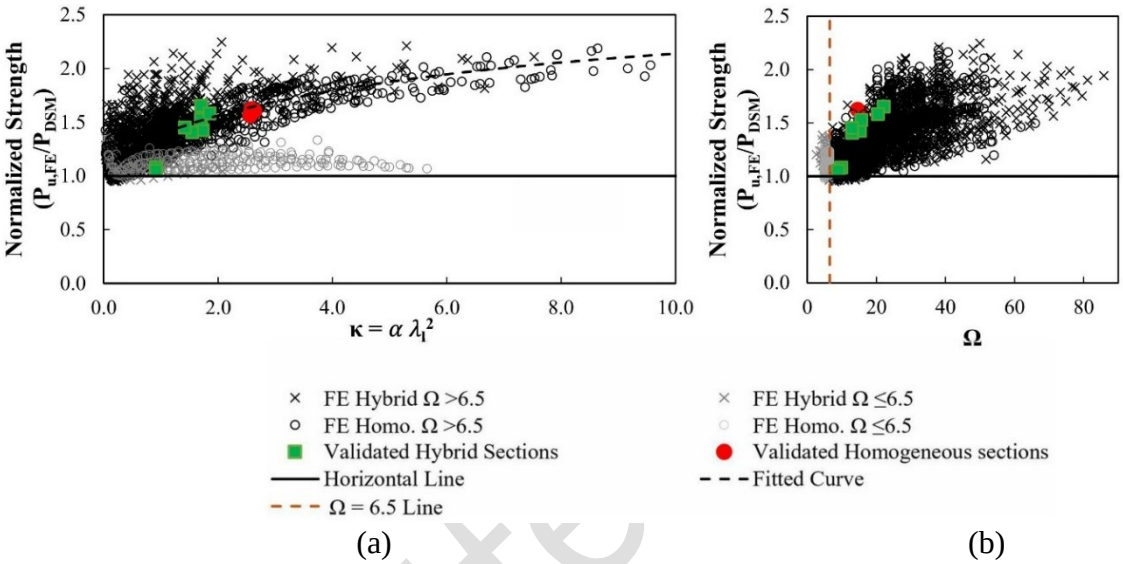
Fitted Curve Equation $g(\alpha, \lambda_l)$	R^2	ϕ		**Mean** $\frac{P_{u,FE}}{P_{mDSM}}$	$\frac{P_{u,FE}}{\phi P_{mDSM}}$	**Section Count**	
		Homo.	**Hybrid**			$P_{u,FE} < P_{mDSM}$	$P_{u,FE} < \phi P_{mDSM}$
$1+1.07\left(1-e^{-0.40\kappa}\right)^{2.19}$ [LB]	-0.25	1.03	1.03	1.202	1.16	69	179
$1+\left(1-e^{-0.49\kappa}\right)^{2.65}$ [LB]	-0.31	1.04	1.04	1.208	1.17	64	184
$1+\left(1-e^{-0.42\kappa}\right)^{2}$ [LB]	-0.14	1.03	1.03	1.191	1.16	77	176
$1+1.30\left(1-e^{-0.14\kappa}\right)^{0.57}$	0.61	0.91	0.95	1.076	1.16	684	161
$1+\left(1-e^{-0.28\kappa}\right)^{0.64}$	0.61	0.91	0.95	1.076	1.16	673	164
$1+\left(1-e^{-0.91\kappa}\right)^{2}$	0.41	0.91	0.98	1.093	1.16	632	159
$-0.86e^{-0.64\kappa}+1.86$	0.58	0.91	0.96	1.079	1.16	651	151
$-0.43e^{-1.5\kappa}+0.08\kappa+1.43$	0.60	0.91	0.96	1.078	1.16	663	164
$1+0.40\kappa^{0.5}$	0.61	0.91	0.95	1.077	1.16	677	167
$1+\frac{0.42\kappa^{0.6}}{1+0.04\kappa}$ **(Selected, Eq. 15)**	0.62	0.91	0.95	1.073	1.16	712	148

The strength reduction factor ϕ was calculated for each of the tested equations, following a procedure described in detail in Section 5. Equations were evaluated based on their R^2 value for this dataset, average prediction accuracy, and the number of unconservative observations. The preferred function $g(\alpha, \lambda_l)$is one that has a strong fit to the data, leads to a strength reduction factor reasonably close to 1.0, and is most algebraically simple. The selected fitted curve outperforms all alternatives, showing the lowest mean error and COV (see Table 7).

Scatter remains in the dataset due to the combined effects of material nonlinearity and geometric variability (leading to the R^2 value 0.62), which are inherent to the problem and not fully captured by our compact analytical expression. Nevertheless, the proposed formulation provides a substantial improvement over the existing DSM-based approach. It provides the lowest mean normalised prediction and achieves markedly reduced scatter with

Submitted copy

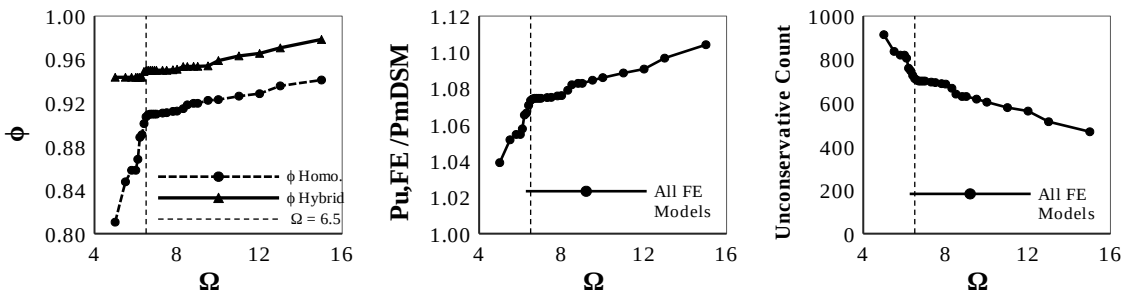
only minor additional analytical complexity for the designer. In addition, it results in the smallest number of unconservative predictions after application of the resistance factor. The selected fitting is plotted amongst the numerical and test data in Figure 7(a). Figure 7(b) shows the normalized capacities versus Ω with a plain line at $\Omega=6.5$ demarcating the limit between strong flange and conventional sections.



(a) (b)

Figure 7. (a) Regression analysis to establish empirical relationship between $P_{u,FE}/P_{DSM}$ and κ (b) $P_{u,FE}/P_{DSM}$ versus Ω with a threshold line at Ω =6.5.

After selecting the correction function, the parameter Ω was re-confirmed. This threshold value separates strong flange from conventional I-sections and is set by evaluating performance of the modified DSM at 28 possible values of Ω in the range $5 \le \Omega \le 15$. Trade-offs were considered between the resistance factor, design accuracy, and conservativeness. The effect of threshold Ω on these three parameters is shown in Figure 8, with an annotated line at Ω=6.5.



Submitte

Figure 8. The effect of the threshold Ω on the resistance factor, average accuracy, and conservativeness of the proposed DSM equation.

Based on this analysis, the original $\Omega = 6.5$ was kept as the optimal threshold (as proposed in Section 3.2). This point marks the onset of reduced slope in each graph, meaning that $\Omega = 6.5$ achieves the greatest possible accuracy without causing a rapid decrease in conservativeness. Figure 7 visually demonstrates that a threshold $\Omega = 6.5$ is effective for separating the clusters of points associated with strong flange and conventional behaviours. Combining the correction function and Ω produces the final set of mDSM equation (*Eq. 16*) which will now assessed in detail in the same way as the three other codified methods.

$$P_{nLG} = \begin{cases} if\ \lambda_l \le 0.776 \quad P_{ne} \\ if\ \lambda_l > 0.776 \cdot \begin{cases} \left(\lambda_l^{-0.8} - 0.15\,\lambda_l^{-1.6}\right) P_{ne}\ if\ \Omega \le 6.5 \\ \left(\left(1 + \dfrac{0.42\,\alpha^{0.6}\,\lambda_l^{1.2}}{1 + 0.04\,\alpha\,\lambda_l^{2}}\right)\left(\lambda_l^{-0.8} - 0.15\,\lambda_l^{-1.6}\right)\right) P_{ne} \le P_y\ if\ \Omega > 6.5 \end{cases} \end{cases} \tag{16}$$

Figure 6(d) depicts the performance of the proposed mDSM method against the numerically computed dataset. The CoV for strong flange sections which was initially 0.19 is reduced by 37% compared to the original DSM predictions, indicating markedly lower variability and improved accuracy in capacity estimates. The average $P_{u,FE}/P_{mDSM}$ ratio indicates that the proposed design modification enhances prediction accuracy by at least 22%. For sections categorized as strong flange sections, the average ratio of numerically computed strength-to-codified DSM prediction was previously 1.38 and is now substantially improved to 1.07 when using the proposed method.

5. Reliability Assessment

The performance of the proposed design equations was assessed in accordance with the reliability assessment guidelines in the commentary to Chapter B of AISC 370-21 [3]. The Load and Resistance Factor Design (LRFD) approach is applied throughout this analysis. The

Submitted Copy

resistance factor ϕ required for the mDSM is calculated per *Eq. 17*, which is a function of two variable types: (1) established basic variables describing material and geometric characteristics of steel members and (2) performance data for the design method evaluated against a sample of numerical or experimental evidence.

In *Eq. 17*, the mechanical factor M_m is the average ratio of measured and specified yield strengths for members in the given material family; the fabrication factor F_m is the average ratio of measured and specified geometrical dimensions; P_m is the ratio of numerically computed failure loads-to-predicted failure loads (with the proposed design method) from the relevant dataset; β is the target reliability index, set at 2.6 for members, targeting a 0.47% probability of failure; V_Q is the CoV of load effects, assuming a dead-to-live load ratio of 3:1; V_R is the CoV of resistance, which is a function of the variation of mechanical properties, geometry, and prediction errors, as per *Eq. 18*.

$$\phi = \frac{1.481 M_m F_m P_m}{\exp\left(\beta \sqrt{V_R{}^2 + V_Q{}^2}\right)} \tag{17}$$

$$V_R = \sqrt{V_M{}^2 + V_F{}^2 + V_P{}^2} \tag{18}$$

Most parameters in this equation are provided in the code based on meta-assessments drawing from large samples of experimental data on stainless steel members. The values of the parameters used in this assessment are given in Table 6. For the average and CoV of mechanical properties (M_m and V_M), different values are given in the code [3] for the austenitic and duplex families of stainless steel and in [55] for carbon steel. P_m and V_P must be calculated by comparing the design method to the numerically computed ultimate strengths and are, therefore, specific to the dataset under consideration.

Table 6. Reliability assessment parameters for steel members.

β	M_m	F_m	P_m	V_R	V_M	V_F	V_P	V_Q
2.6	1.25 (A) 1.10 (D)	1.00	Data Dependant	$\sqrt{V_M{}^2 + V_F{}^2 + V}$	0.08 (A) 0.04 (D)	0.05	Data Dependant	0.19

Submitted Copy

	1.10 (C)	0.10 (C)

Mechanical properties have different averages and CoVs in different families of stainless steel. (A) indicates austenitic stainless steel, (D) indicates duplex and (C) indicates carbon steel.

Because the code provides different basic variables for different stainless steel, it is possible to calculate different resistance factors for each family. However, when resistance factors for design methods are specified in the stainless steel code [3], one overall ϕ factor is provided. In this study, two separate ϕ - one for homogeneous sections and one for hybrid sections – are calculated by taking the more conservative basic variable for each parameter and applying these to the respective datasets separately. That is, taking 1.10 for M_m and 0.08 for V_M for the overall homogeneous sections, and taking 1.10 for M_m and 0.1 for V_M for hybrid sections. Figure 9 shows the resistance factor results of mDSM evaluated at 28 different threshold values for Ω. The same general trend that was shown in Figure 8 is preserved when calculating the resistance factor separately, the "Overall homogeneous" curve being the most conservative, as expected.

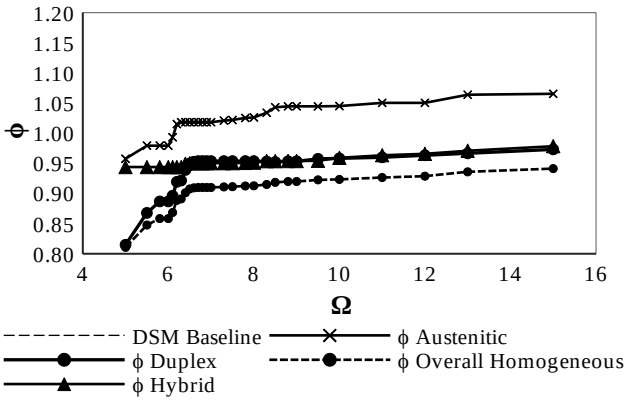


Figure 9. Resistance factor ϕ versus Ω threshold for multiple stainless steel families.

The DSM baseline set at $\phi = 1.03$ in Figure 9 was determined by calculating the resistance factor per *Eq. 17* for the codified DSM based on our numerical dataset. As a basis of comparison, the LRFD resistance factor $\phi = 0.85$ is given for the DSM in AISI S100-16 (2020) Section E3 [43]. The "Overall" ϕ value of 0.91 for homogeneous sections and 0.95 for hybrid sections was calculated for the mDSM at the selected Ω threshold of 6.5, which it

Submitted Copy

615 as lower than the calculated DSM baseline for this dataset, but still safely above the 0.85
616 value given in the code.

617 The number of unconservative observations in the mDSM design strength analysis is
618 unusually high, representing a 5.8% probability of failure compared to the target probability
619 of 0.47%. This observation is related to the finding that the ϕ value calculated based on this
620 dataset is higher than the codified resistance factor. The unique characteristics of this
621 numerical dataset – including its focus on high slenderness and strong flange sections – likely
622 render it unrepresentative of the datasets typically used to evaluate general compression
623 members. The high calculated values of ϕ are a substantial influence leading to the high
624 number of unconservative observations.

625 The plots in Figure 10 report the distribution of numerically computed strengths
626 divided by the predicted strengths. The histograms in Figure 10 are overlayed with normal
627 distributions defined by the mean and standard deviation of the data. The performance of the
628 calculated ϕ value of 0.91 for homogeneous sections or 0.95 for the hybrid group of sections
629 and codified $\phi = 0.85$ are demonstrated. One of the core assumptions invoked in reliability
630 assessment is that variation in load and resistance effects is normally distributed [43, 3].
631 While dataset used here is large, the numerically computed-to-predicted strength errors have
632 a right skew.

633 In the nominal case, P_{mDSM} returns an average error term P_m of 1.073 with a standard
634 deviation of 0.13. The nominal strength prediction is unconservative for 29% of the dataset.
635 The design strength with ϕ as 0.91 for homogeneous sections or 0.95 for the hybrid group of
636 sections returns an average of 1.16 and standard deviation of 0.13, with a mere 5.8%
637 unconservative observations. Finally, the design strength with the codified ϕ of 0.85 returns a
638 mean of 1.26 and 0.15 as standard deviation, and only 0.7% unconservative results.

Submitted Copy

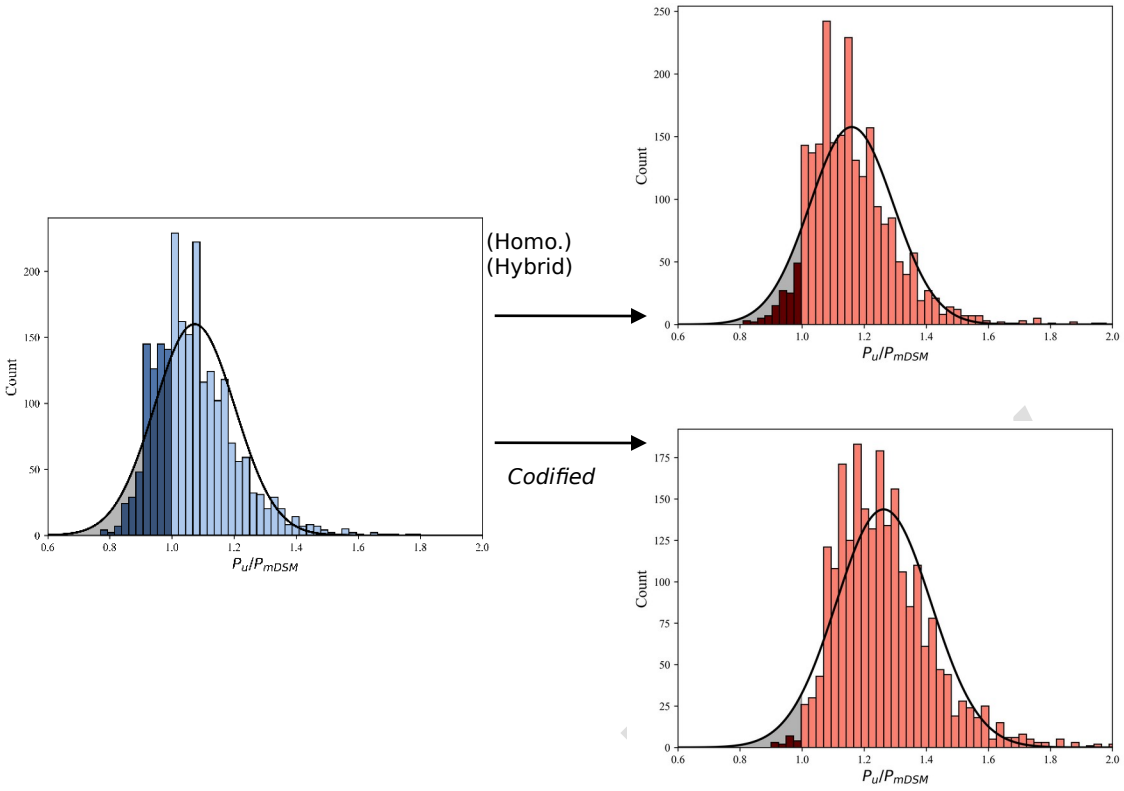


Figure 10. Distribution of numerically computed-to-predicted strength ratios based on ϕ values.

This reliability analysis gives strong evidence that the proposed mDSM method is applicable with the same resistance factor that is currently used in the American code for the DSM [43]. The dataset nearly fulfils the assumption of normally distributed variation, with only a slight skew. The skew is caused mostly by the inclusion of sections in the low slenderness range that develop loads far above their yield capacity and has very minimal impact on reliability results. If the skew were removed from the dataset, the average observed P_u/P_{mDSM} would slightly decrease, and the probability of failure would remain the same, resulting in an extremely small decrease in the calculated value of ϕ. The 0.7% probability of failure observed for this dataset when using the codified ϕ of 0.85 is within reasonable vicinity of the targeted probability of failure – approximately 0.47% in the case of a standard normal cumulative distribution – based on a β of 2.6 given in the American code [3] for members.

Submitted

6. Conclusions

Numerical and experimental evidence from the past twenty years has suggested the existence of a distinct strong flange behaviour, where I-sections with flanges substantially stronger than the web can develop compressive strengths much greater than some existing design predictions. Research on carbon steel [6] posited that the I-profile web developed its local buckling capacity while the flanges approached their full plastic capacity with minimal deformation before failure. This phenomenon is termed strong flange behaviour.

This research demonstrates that strong flange behaviours are not well accounted for by existing design methods. This is particularly true when members have plates of different slenderness, and the design method (e.g. DSM and CSM) considers a whole-section definition of slenderness. The new design approach proposed in this paper aimed to address the oversights of "whole section" design methods without entirely sacrificing their marked advantage of simplicity.

A detailed FE model was developed and validated against experimental results in a companion paper by the same authors [7]. The validated model was extended to conduct a comprehensive parametric study considering a wide range of geometric parameters and four stainless steel grades, two austenitic and two duplex. A total of 2280 stub column compression tests were modelled, including both strong flange and conventional I-sections.

Strength predictions from three codified design methods – the EWM, DSM, and CSM – were compared with the numerical results. The comparison demonstrated that strong flange behaviour is a characteristic affecting design accuracy in all three methods. Among these methods, the current EWM predicts the capacity of strong flanges sections most accurately. The DSM and CSM give conservative predictions with high variation for the strength of strong flange I-sections, and the DSM is generally accurate for non-strong flange sections.

Submitted Copy

A modified DSM was developed to identify sections likely to exhibit strong flange behaviour and predict the effect on ultimate strength. Two new parameters, Ω and α were included in the new mDSM formulation to distinguish between behaviours and quantify ultimate strengths more accurately. The proposed mDSM was evaluated against the numerical data and was shown to provide predictions with much greater accuracy and lower variation among the considered methods.

A reliability assessment indicates that the existing DSM codified ϕ value of 0.85 applied to the new mDSM equation ensures a robust level of safety across the full range of slenderness. The proposed mDSM preserves most of the simplicity of the codified DSM, while introducing two simple parameters that are sufficient to account for the effects of strong flange behaviour in stainless steel I-sections under pure compression.

Data Availability Statement

All data, models, and code generated or used during the study appear in the submitted article.

Acknowledgements

Usman Ali is a doctoral candidate whose research and studies are funded by the Marie Sklodowska-Curie Doctoral Network (MSCA-DN) SeaChem project, EU Grant No. 101073471. Gregory Langone is an Engineer Officer in the U.S. Army and a recipient of the John & Daria Barry Scholarship which generously supports his studies. The authors also gratefully acknowledge Majid Shamlooei for his help in the initial FE model development.

References

[1] CEN (Committee of European Normalization), Eurocode 3: Design of steel structures - Part 1-4: General rules and supplementary rules for stainless steels (EN 1993-1-4), Brussels, 2006.

[2] Joint Technical Committee BD-082, Cold-formed Steel Structures, “AS/NZS 4600:2005 Cold-formed steel structures,” Sydney, 2005.

[3] American Institute of Steel Construction (AISC), “ANSI/AISC 370-21: Specification for Structural Stainless Steel Buildings,” 2021.

[4] ANSI/AISC, “360-22 Specification for Structural Steel Buildings,” 2022.

Submitted Copy

[5] M. Seif and B. W. Schafer, “Local buckling of structural steel shapes,” *Journal of Constructional Steel Research,* vol. 66, no. 10, pp. 1232-1247, October 2010.

[6] B. Rossi and Y. Li, “Extension of the DSM to welded H profile cross-sections,” in *Research and Applications in Structural Engineering, Mechanics and Computation*, 2013, pp. 1291-1296.

[7] G. Langone, M. Shamlooei, U. Ali, X. Ruan and B. Rossi, “Extension of the direct strength method to fabricated I-profiles under compression,” in *Nordic Steel Construction Conference*, Lulea, Sweeden, 2024.

[8] S. Chen, J.-z. Liu and T.-M. Chan, “Investigations into the local buckling and post-buckling behaviour of fixed-ended hybrid I-section stub columns with slender web,” *Thin-Walled Structures,* vol. 184, 2023.

[9] R. W. Frost and C. . G. Schilling, “Behavior of hybrid beams subjected to static loads,” *Journal of the Structural Division,* vol. 90, no. 3, pp. 55-88, 1964.

[10] P. S. Carskaddan, “Shear buckling of unstiffened hybrid beams,” vol. 94, no. 8, p. Journal of the Structural Division, 1968.

[11] N. . N. R. Rao, “The strength of hybrid steel columns,” Department of Civil Engineering, Lehigh University, Pennsylvania, 1965.

[12] J.-z. Liu, C. Shuxian and C. Tak-Ming, “Experimental and numerical investigations of hybrid high strength steel welded T-section stub columns with Q690 flange and Q460 web,” *Thin-Walled Structures,* vol. 177, 2022.

[13] G. Langone, U. Ali and B. Rossi, “[Under Review] Tests of hybrif stainless steel I-profile columns under pure compression,” *ASCE Journal of Structural Engineering,* 2025.

[14] R. Lalthazuala and K. Singh, “Structural behaviour of hybrid stainless steel stub columns under axial compression,” *Structures,* vol. 27, pp. 128-140, October 2020.

[15] M. Bock, M. Gkantou, M. Theofanous, S. Afshan and H. Yuan, “Ultimate behaviour of hybrid stainless steel cross-sections,” *Journal of Constructional Steel Research,* vol. 210, 2023.

[16] N. Saliba and L. Gardner, “Cross-section stability of lean duplex stainless steel welded I-sections,” *Journal of Constructional Steel Research,* vol. 80, pp. 1-14, January 2013.

[17] K. Jiang, Zhao and Ou, “Stainless steel built-up section stub columns: Testing, numerical modelling and design,” *Thin-Walled Structures,* vol. 191, October 2023.

[18] G. Shu, S. Yang, X. Jin, S. Dong, Q. Jiang and B. Zheng, “Study on the bearing capacity of S600E high-strength stainless steel welded cross-sections,” *Journal of Constructional Steel Research,* vol. 175, December 2020.

[19] L. Gardner, Y. Bu and M. Theofanous, “Laser-welded stainless steel I-sections: Residual stress measurements and column buckling tests,” *Engineering Structures,* vol. 127, pp. 536-548, November 2016.

[20] H. Yuan, Y. Wang, L. Gardner, X. Du and Y. Shi, “Local–overall interactive buckling behaviour of welded stainless steel I-section columns,” *Journal of Constructional Steel Research,* vol. 111, pp. 75-87, 2015.

[21] H. Ran, Z. Chen and Y. Ma, “Experimental and numerical studies of laser-welded slender stainless steel I-section columns,” *Thin-Walled Structures,* vol. 171, 2022.

[22] M. Theofanous and L. Gardner, “Testing and numerical modelling of lean duplex stainless steel hollow section columns,” *Engineering Structures,* vol. 31, no. 12, pp.

Submitted Copy

3047-3058, December 2009.
[23] H. Yuan, Y. Wang, Y. Shi and L. Gardner, “Stub column tests on stainless steel built-up sections,” *Thin-Walled Structures,* vol. 83, pp. 103-114, October 2014.
[24] L. Yang, M. Zhao, D. Xu, F. Shang, H. Yuan, Y. Wang and Y. Zhang, “Flexural buckling behavior of welded stainless steel box-section columns,” *Thin-Walled Structures,* vol. 104, pp. 185-197, 2016.
[25] L. Gardner, A. Talja and N. Baddoo, “Structural design of high-strength austenitic stainless steel,” *Thin-Walled Structures,* vol. 44, no. 5, pp. 517-528, May 2006.
[26] B. Young and Y. Liu, “Experimental Investigation of Cold-Formed Stainless Steel Columns,” *Journal of Structural Engineering,* vol. 129, no. 2, January 2003.
[27] J. Becque and K. Rasmussen, “Experimental investigation of local-overall interaction buckling of stainless steel lipped channel columns,” *Journal of Constructional Steel Research,* vol. 65, no. 8-9, pp. 1677-1684, August-September 2009.
[28] K. Sachidananda and K. D. Singh, “Numerical study of fixed ended lean duplex stainless steel (LDSS) flat oval hollow stub column under pure axial compression,” *Thin-Walled Structures,* vol. 96, pp. 105-119, November 2015.
[29] A. Salem, M. El Aghoury, F. El Dib and M. Hanna, “Post local buckling strength of bi-axially loaded slender I-section columns,” *Thin-Walled Structures,* vol. 43, no. 7, pp. 1003-1019, July 2005.
[30] A. J. Davids and G. J. Hancock, “Compression Tests of Short Welded I-Sections,” *Journal of Structural Engineering,* vol. 112, no. 5, 1986.
[31] H. Kuwamura, “Local Buckling of Thin-Walled Stainless Steel Members,” *Steel Structures,* pp. 191-201, 2003.
[32] A. Su, Y. Sun, Y. Liang and O. Zhao, “Membrane residual stresses and local buckling of S960 ultra-high strength steel welded I-section stub columns,” vol. 161, 2021.
[33] F. Zhou, L. Tong and Y. Chen, “Experimental and numerical investigations of high strength steel welded h-section columns,” *International Journal of Steel Structures,* 2013.
[34] K. Rasmussen and G. Hancock, “Plate slenderness limits for high strength steel sections,” *Journal of Constructional Steel Research,* vol. 23, no. 1-3, pp. 73-96, 1992.
[35] Dassault Systems Simulis Corp, “ABAQUS/CAE User's Manual,” Providence, RI, 2022.
[36] S. Chen, J.-z. Liu and T.-M. Chan, “Local buckling behaviour of high strength steel and hybrid I-sections under axial compression: Numerical modelling and design,” *Thin-Walled Structures,* vol. 191, 2023.
[37] CEN(European Committee for Standardization), “Eurocode 3: Design of steel structures – Part 1-1: General rules and rules for buildings (EN 1993-1-1:2005),” Brussels, 2006.
[38] B. Nancy, Design Manual for Structural Stainless Steel (4th Edition), Ascot, United Kingdom: Steel Construction Institute (SCI), 2017.
[39] CEN (Committee of European Normalization), Eurocode 3: Design of steel structures - Part 1-5: General rules - Plated structural elements. (EN 1993-1-5), Brussels, 2006.
[40] S. Chen, J.-z. Liu and T.-M. Chan., “Material properties and residual stresses of welded high strength steel and hybrid I-sections,” *Engineering Structures,* vol. 276.

Submitted copy

[41] CEN (European Committee for Standardization), "prEN 1993-1-14: Eurocode 3 – Design of steel structures – Part 1-14: Design assisted by finite element analysis," CEN, Brussels, 2023.
[42] H. Yuan, Y. Wang, Y. Shi and L. Gardner, "Residual stress distributions in welded stainless steel sections," *Thin-Walled Structures,* vol. 79, pp. 38-51, June 2014.
[43] AISI, "S100-16: North American Specification for the Design of Cold-Formed Steel Structural Members," American Iron and Steel Institute, 2020.
[44] L. Gardner, A. Fieber and Macorini, "Formulae for Calculating Elastic Local Buckling Stresses of Full Structural Cross-sections," *Structures,* vol. 17, pp. 2-20, February 2019.
[45] B. Rossi and K. Rasmussen, "Carrying Capacity of Stainless Steel Columns in the Low Slenderness Range," *Journal of Structural Engineering,* vol. 139, no. 6, 28 May 2012.
[46] B. W. Schafer and T. Pekoz, "Direct Strength Prediction of Cold-formed Steel Members Using Numerical Elastic Buckling Solutions," in *CCFSS Proceedings of International Specialty Conference on Cold-Formed Steel Structures,* 1998.
[47] B. Schafer, "Progress on the Direct Strength Method," in *CCFSS Proceedings of International Specialty Conference on Cold-Formed Steel Structures,* 2002.
[48] L. Gardner, "The continuous strength method," *Proceedings of the Institution of Civil Engineers - Structures and Buildings,* vol. 161, no. 3, pp. 127-133, June 2008.
[49] ASCE, "Specification for the Design of Cold-Formed Stainless Steel Structural Members," American Society of Civil Engineers , Reston, Virginia, 2021.
[50] M. Ashraf, L. Gardner and D. Nethercot, "Structural Stainless Steel Design: Resistance Based on Deformation Capacity," *ASCE Journal of Structural Engineering,* vol. 134, no. 3, 2008.
[51] S. Afshan and L. Gardner, "The continuous strength method for structural stainless steel design," *Thin-Walled Structures,* vol. 68, pp. 42-49, July 2013.
[52] A. Liew and L. Gardner, "Ultimate capacity of structural steel cross-sections under compression, bending and combined loading," *Structures,* vol. 1, pp. 2-11, 2015.
[53] O. Zhao, S. Afshan and L. Gardner, "Structural response and continuous strength method design of slender stainless steel cross-sections," *Engineering Structures,* vol. 140, pp. 14-25, June 2017.
[54] L. Gardner, X. Yun and F. Walport, "The continuous strength method–review and outlook," *Engineering Structures,* vol. 275, 2023.
[55] L.-E. Hsiao, W.-W. Yu and T. V. Galamb, "AISI LRFD method for cold-formed steel structural members," *Journal of Structural Engineering,* vol. 116, pp. 500-517, 1990.

699
700

Submitted Copy

Appendix

Built-up I-section stub column test data collected from literature, including measured geometries, measured material properties, and ultimate loads. Data source articles are listed in Table 1 and used to produce Figure 2 and 4.

- Section ID indicates the label given to each section in the source publication.
- In the material column, “A” represents austenitic stainless steel, “D” represents duplex stainless steel, and “CS” represents carbon steel (including high strength grades).

Reference	Section ID	Material	L [mm]	h_w [mm]	b [mm]	t_w [mm]	t_f [mm]	$f_{y,\,web}$ [MPa]	$f_{y,\,flange}$ [MPa]	E [MPa]	P_u [kN]
[21]	I-120×60×4×4	A	360	111.7	59.9	3.83	3.82	300	300	192500	274
	I-140×80×3×3	A	420	134.2	79.7	2.75	2.74	291	291	185000	174
	I-90×60×3×3	A	270	84.3	60.3	2.80	2.81	291	291	185000	173
	I-90×60×4×4	A	270	81.6	59.8	3.83	3.83	300	300	192500	266
	I-120×90×3×3	A	360	113.7	90.0	2.78	2.78	297	297	189000	196
	I-100×80×3×3	A	200	93.7	79.5	2.75	2.74	291	291	185000	173
	I-140×140×3×3	A	421	133.8	139.2	2.75	2.74	291	291	185000	211
	I-90×90×3×3	A	270	83.9	89.7	2.77	2.77	297	297	189000	179
	I-60×60×3×3	A	180	54.7	60.2	2.78	2.78	297	297	189000	163
[31]	SC-2H1	A	150	45.0	49.9	2.96	2.96	249	249	203000	153
	SC-2H2	A	300	44.1	98.9	2.94	2.94	249	249	203000	193
	SC-2H3	A	300	95.4	49.7	2.93	2.93	249	249	203000	171
	SC-2H4	A	300	95.4	75.2	2.93	2.93	249	249	203000	200
	SC-2H5	A	300	95.4	99.7	2.92	2.92	249	249	203000	203
	SC-2H6	A	450	145.0	99.6	2.95	2.95	249	249	203000	208
	SC-2H7	A	600	194.8	100.2	2.93	2.93	249	249	203000	206
	SC-2H8	A	600	195.2	150.4	2.95	2.95	249	249	203000	231
	SC-4H1	A	150	45.2	49.3	3.01	3.04	497	497	206000	253
	SC-4H2	A	300	45.6	99.2	3.01	2.99	497	497	206000	290
	SC-4H3	A	300	95.2	50.3	3.01	3.03	497	497	206000	280
	SC-4H4	A	300	96.0	74.8	2.99	3.02	497	497	206000	310
	SC-4H5	A	300	94.3	99.7	3.02	3.02	497	497	206000	323
	SC-4H6	A	450	145.2	99.5	3.02	3.02	497	497	206000	310
	SC-4H7	A	600	195.9	100.1	3.02	3.01	497	497	206000	311
	SC-4H8	A	600	195.4	149.8	3.01	3.02	497	497	206000	360
[19]	I-300×150×7×11	A	840	271.5	150.5	6.92	11.81	237	290	198550	1672
	I-220×110×6×9	A	660	201.8	110.4	6.07	8.91	275	292	195100	1072
	I-150×75×7×10	A	450	130.7	75.8	7.05	9.90	274	267	197250	854
	I-160×82×10×12	A	480	136.5	83.2	9.79	11.72	264	286	198000	1398
	I-203×133×6×8	A	612	189.4	133.9	5.90	7.83	251	281	192500	1090
	I-102×68×5×5	A	305	91.6	68.0	5.01	5.11	222	222	186800	430
	I-152×160×6×9	A	456	134.7	160.6	6.18	8.79	272	227	198050	1163
	I-140×140×10×12	A	420	116.1	140.8	9.71	11.82	260	272	190250	2042
	I-50×50×4×4	A	150	42.5	50.5	3.99	3.91	270	270	190700	281
[20]	I304-492-i	A	2138	482.9	198.0	6.00	6.00	316	316	195250	737
	I304-432-i	A	2037	422.1	173.5	6.00	6.00	316	316	195250	717
	I304-372-i	A	2889	361.1	245.5	6.00	6.00	316	316	195250	894
	I304-312-i	A	3137	301.3	305.0	6.00	6.00	316	316	195250	991
	I304-252-i	A	2938	240.7	245.5	6.00	6.00	316	316	195250	843
	I2205-492-i	D	2141	481.8	196.9	6.00	6.00	651	651	207200	1256
	I2205-432-i	D	2039	422.1	172.9	6.00	6.00	651	651	207200	1015
	I2205-372-i	D	2887	362.0	245.0	6.00	6.00	651	651	207200	1322
	I2205-252-i	D	2935	241.3	245.0	6.00	6.00	651	651	207200	1290
	I2205-312-i	D	3140	301.1	305.0	6.00	6.00	651	651	207200	1445
[16]	I-200x140x6x6	D	600	202.1	138.9	6.01	6.12	516	516	200000	1473
	I-200x140x8x6	D	600	201.1	139.0	5.98	8.04	516	504	200000	1849
	I-200x140x10x8	D	600	199.2	139.0	8.03	10.35	504	501	200000	2540
	I-200x140x12x8	D	600	199.1	139.3	8.14	12.68	504	456	200000	2978
[8]	H440-460W	CS	500	420.3	109.7	6.30	9.70	521	820	215800	2422
	H440-690W	CS	499	420.2	110.1	6.30	9.60	789	820	216100	2887
	H440-355W	CS	499	419.6	110.1	6.70	9.50	402	820	220000	2363
	H350-690W	CS	400	329.2	109.8	6.50	9.50	789	820	216100	2802
	H350-460W	CS	396	330.1	110.4	6.60	9.60	521	820	215800	2445
	H350-355W	CS	296	329.3	110.0	6.80	9.70	402	820	220000	2371
	H230-690W-L1	CS	252	207.8	110.3	6.20	9.80	789	820	216100	2674
	H230-690W-L2	CS	462	208.1	110.8	6.40	9.60	789	820	216100	2641

Submitted Copy

	H230-460W-L1	CS	251	207.5	109.9	6.60	9.70	521	820	215800	2458
	H230-460W-L2	CS	462	208.7	109.8	6.60	9.60	521	820	215800	2378
	H230-355W-L2	CS	462	209.3	110.0	6.70	9.70	402	820	220000	2302
	H230-355W-L1	CS	251	209.1	109.6	6.80	9.70	402	820	220000	2369
[30]	190-3	CS	895	190.1	190.0	5.00	5.00	411	411	202000	932
	190-1	CS	895	190.1	190.0	5.00	5.00	411	411	202000	933
	240-2	CS	1095	241.1	240.0	5.00	5.00	411	411	202000	1000
	240-1	CS	1095	241.1	240.0	5.00	5.00	411	411	202000	995
	310-2	CS	1395	311.0	310.0	5.00	5.00	411	411	202000	1104
	310-1	CS	1395	311.0	310.0	5.00	5.00	411	411	202000	1087
[32]	I-150×75×6-1	CS	321	137.5	75.9	6.14	6.14	972	972	203341	1621
	I-150×75×6-2	CS	320	136.9	76.0	6.10	6.10	972	972	203341	1671
	I-200×150×6-1	CS	599	187.7	149.7	6.01	6.01	972	972	203341	2223
	I-200×150×6-2	CS	600	188.1	150.0	5.96	5.96	972	972	203341	2080
	I-80×60×6-2	CS	210	67.1	59.3	5.96	5.96	972	972	203341	1217
	I-80×60×6-1	CS	209	66.9	59.2	6.03	6.03	972	972	203341	1251
	I-90×70×6-2	CS	240	78.5	69.5	6.01	6.01	972	972	203341	1405
	I-90×70×6-1	CS	239	77.8	69.2	5.97	5.97	972	972	203341	1394
	I-150×150×6-1	CS	449	137.4	149.2	5.98	5.98	972	972	203341	2104
	I-150×150×6-2	CS	450	137.4	150.0	6.07	6.07	972	972	203341	2180
	I-120×120×6-1	CS	359	107.2	119.3	5.99	5.99	972	972	203341	2136
	I-120×120×6-2	CS	361	106.9	119.6	6.03	6.03	972	972	203341	1930
	I-70×70×6-2	CS	211	58.1	69.3	5.94	5.94	972	972	203341	1264
	I-70×70×6-1	CS	209	57.8	69.3	6.01	6.01	972	972	203341	1300
	I-50×50×6-1	CS	148	37.9	49.2	5.98	5.98	972	972	203341	951
	I-50×50×6-2	CS	149	37.0	49.2	6.06	6.06	972	972	203341	947
[34]	I3SC1	CS	450	180.0	136.0	6.00	6.00	725	725	211000	1706
	I2SC1	CS	400	150.0	116.0	6.00	6.00	725	725	211000	1590
	I1SC1	CS	350	120.0	96.0	6.00	6.00	725	725	211000	1367
[33]	H300×200×12×12	CS	798	300.8	199.8	12.66	12.66	516	516	200000	5309
	H300×200×10×10	CS	800	301.0	199.3	10.23	10.23	550	550	280100	4461
[29]	L1-15-120	CS	1001	601.0	74.0	4.95	4.95	322	322	202963	721
	L2-14-80	CS	2001	401.0	71.0	4.90	4.80	322	322	202963	618
	L1-15-80	CS	999	309.0	77.0	4.80	4.80	322	322	202963	746
	L2-24-120	CS	1999	399.0	119.0	5.10	5.10	322	322	202963	721
	L2-24-80	CS	1999	399.0	121.0	4.93	4.93	322	322	202963	783

708

Submitted Copy